Results in Engineering 24 (2024) 102933

Contents lists available at ScienceDirect

Results in Engineering

journal homepage: www.sciencedirect.com/journal/results-in-engineering

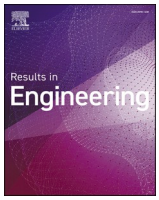

The effects of graphene oxide nanoparticles on the mechanical and thermal properties of polyurethane/polycaprolactone nanocomposites; a molecular dynamics approach

Shapour Fadaei Heydari, Mohamad Shahgholi *, Arash Karimipour, Mehdi Salehi, Seyed Ali Galehdari

Department of Mechanical Engineering, Najafabad Branch, Islamic Azad University, Najafabad, Iran

A R T I C L E I N F O

Keywords:
Smart polymer
Graphene oxide
Polycaprolactone
Mechanical properties
Molecular dynamics simulation

A B S T R A C T

Using molecular dynamics simulations using LAMMPS and other tools, this work examined the effect of graphene oxide nanoparticles on the mechanical and thermal properties (TPs) of polyurethane/polycaprolactone nanocomposites. The simulations examined the atomic, MP, and thermodynamic properties of atomic structures while examining and equilibrating them. After 10 ns of equilibration at 300 K and 1 bar, samples were convergent and the simulation parameters were confirmed. The addition of GO-NPs significantly enhanced TPs and MPs, with optimal improvements observed at a 2 % concentration. Specifically, increasing GO-NP content from 0.5 % to 2 % resulted in increases in heat flux from 680.95 to 714.09 W/m^2, thermal conductivity from 0.69 to 0.93 W/m·K, and Young's modulus from 5.91 to 6.63 MPa. This is while increasing GO-NP content from 0.5 % to 2 % resulted in decreases in both the mean square displacement and glass transition temperature (Temp) to 0.22 Å^{2}and 318 K, respectively. However, further increasing the GO-NP concentration to 5 % led to a decrease in HF and TC, likely due to nanoparticle agglomeration, which also reduced mechanical strength and increased MSD and Tg. This study underscores the importance of optimizing GO-NP concentration, with 2 % identified as the most effective for enhancing the properties of PU/PCL/GO-NCs.

Nomenclature

Glass transition temperature	Hg	Redial Distribution Function	RDF
Graphene Oxide	GO	Shape Memory	SM
Heat flux	HF	Simulation Box	SB
Lennard-Jones	LJ	Smart Polymer	SP
Mechanical Behavior	MB	Temp	Temp
Mechanical Properties	MPs	Thermal Behavior	TB
Mechanical Strength	MS	Thermal Conductivity	TC
Mean Square Displacement	MDS	Thermal Properties	TPs
Molecular Dynamics	MD	Ultimate Strength	US
Nanocomposites	NCs	Volum	Vol
Nanoparticles	NPs	Young's modulus	YM
Polyurethane	PU		
Polycaprolactone	PCL		

1. Introduction

Through the exploration of new materials, humans have successfully created synthetic materials using organic substances found in nature. Polymer materials are compounds of the chemical elements carbon, hydrogen, oxygen, nitrogen, and sulfur. Polymers are chemical compounds consisting of massive molecules structured by repeating components known as monomers. Polymers possess favorable physical and MPs, such as low specific gravity and chemical resistance. Some polymers are even transparent which can be used as a substitute for glass [1–3]. Most polymers act as electrical insulators, although certain types exhibit some degree of electrical conductivity [4,5]. It is possible to detect smart Propertiesin several material groups. SPs show different reactions to external stimuli, such as Temp, magnetic fields, and electric fields. These polymers are divided into many categories based on their unique properties and uses [6–8]. One notable branch of SPs is SM polymers, which have gained significant commercial use. To sustain the required deformation, SM polymers need to be able to create strong

* Corresponding author.
E-mail address: m.shahgholi@pmc.iaun.ac.ir (M. Shahgholi).

https://doi.org/10.1016/j.rineng.2024.102933
Received 21 July 2024; Received in revised form 3 September 2024; Accepted 17 September 2024
Available online 19 September 2024

reversible connections (secondary cross-links) among their polymer components [9–12]. However, SM polymers have lower modulus and rebound stress compared to metal alloys or SM ceramics. Therefore, it is necessary to enhance the properties of these polymers [13]. One solution is to create SM composites by incorporating fillers and NPs into the material [14,15]. Integrating GO NP's into SP systems, particularly SM polymers, offers significant advantages that address the inherent limitations of these materials. Strong interfacial contacts with the polymer matrix are made possible by GO's large surface area, MS, and functional groups. These interactions improve MPs like modulus and rebound stress, which are often lower in SM polymers than in metal alloys or ceramics. Furthermore, GO-NPs improved TC and electrical conductivity, making SM polymers more responsive to external stimuli, such as Temp and electric fields, thereby lowering activation energy and enabling faster shape recovery. Beyond these mechanical and conductive enhancements, GO contributed to improved biocompatibility and biodegradability, particularly in applications involving biodegradable PCL. PCL is a biodegradable polyester that is part of aliphatic polyester group. Ring-opening polymerization of caprolactone (CL) monomers is required for its formation. The linear chain structure of resulting polymer is composed of recurring CL units. PCL gained considerable attention which was extensively used in a variety of applications due to its distinctive qualities and Properties [16].

Razzaghi et al. [17] investigated how the combination of G and GO nanosheets grafted with PCL affects the microstructure, biocompatibility, thermoregulatory properties, and MPs of electrospun PU-NC mats. The results suggest that a wound dressing made of a PU-GPCL electrospun nanofiber mat containing 1 % GPCL nanosheets would be appropriate. Azadi et al. [18] investigated the effect of GO on the Therly induced SM behavior of Polylactic acid (PLA)/PU composites. According to the research, PLA/PU/GO-NCs showed improvements in storage and YM, tensile strength, creep resistance, and creep recovery. Consequently, these materials were amenable to a diverse range of environmentally sustainable applications. Cetiner et al. [19] studied the effect of adding thermoplastic PU and G NPs to PLA on SM behavior, MPs, and TB. According to the findings, adding 0.5 % of G nanoplatelets by weight improved TPs by 15 % and MPs by 24 %. Furthermore, PU was added to PLA at a weight ratio of 9:1, which improved SM and flexibility. Liang et al. [20] studied the effect of incorporating GO-NPs into the PU's MPs and discovered that a 0.70 % weight increase in G NPs resulted in a 64.89 % improvement in the NC's tensile strength. Gupta et al. [21] examined the MPs of SP PCL/cellulose nanocrystals in their study. The results demonstrate that adding cellulose nanocrystals up to 10 % by weight greatly enhanced the tensile strength (from 0.2 to 7.2 MPa), tensile strength at break, and modulus of elasticity (from 3.5 to 139.3 MPa). Saidi et al. [22] focused creating a model to predict the bond strength between Reinforced Polymer sheets and concrete. Various fiber types, including jute and abaca, along with different adhesives, were tested, revealing that increasing fabric layers significantly enhanced bond strength up to 400 %. Samuel and Tayong [23] focused the advantages of using Carbon Fibre Reinforced Polymers for automotive drive shafts, comparing them to traditional materials like steel and aluminum. The results show that these shafts were a viable substitute in automotive applications since they were much lighter, had better mechanical qualities, and showed maximum fatigue resistance. Karim et al. [24] reviews the application of fibre-reinforced polymers in various fields, highlighting their advantages, such as high strength-to-weight ratios and corrosion resistance. Peng et al. [25] explored the effect of Temp on the TPs and MPs of PU/PCL/GO-NCs using MD simulations. Their research demonstrated that when Temp increased to 350 K, HF and TC dropping to 681.85 W/m^2 and 0.82 W/m·K, respectively. Temp increase resulted in an expansion of NCs Vol to 27,364 cubic nanometers. Furthermore, the material's US decreased from 72.59 MPa to 68.22 MPa and its YM decreased from 6.63 MPa to 6.36 MPa when the Temp increased from 300 K to 350 K. Heydari et al. [26] examined how varying the PCL content affects the TPs and MPs of PU/PCL/GO-NCs using MD simulations. Their findings revealed that increasing the PCL content from 10 % to 50 % resulted in higher HF (from 688.43 to 724.03 W/m^2) and TC (from 0.85 to 0.99 W/m·K). Additionally, this increase in PCL content led to improvements in the NP's US (from 56.32 to 62.23 MPa) and YM (from 5.99 to 6.29 MPa). Finally, the MDS and Tg stabilized at 0.31 Å^2 and 331 K, respectively, with higher PCL content. Quanguo et al. [27] explored the interaction properties and mechanical enhancements of thermoplastic PU-NCs reinforced with GO using MD simulations. The researchers used reactive MD simulations to evaluate the ReaxFF coupling field's accuracy in calculating physical properties and MPs of TPU/GO-NCs. The findings of this investigation show that adding 18 wt% GO increased YM by 34 %, from 281 GPa for TPU to 378 GPa for TPU/GO, with considerable charge transfer (3.483 e) from TPU to the GO skeleton.

MD modeling was utilized to analyze SM, MPs, and TPs of an SP-NC composed of PU/PCL/GO. The thermodynamic, TPs, and atomic properties of the NC were assessed in relation to various concentrations of GO-NPs (0.5, 1, 2, and 5 %) using LAMMPS computer software and MD simulation. In fact,the innovation of this study lies in its comprehensive approach, addressing both the optimal GO concentration and the Temp-dependent behavior of NCs. By integrating these aspects, the study provided new insights into effectively balancing TPs and MPs. It set the stage for future experimental validation, addressing the gap between theoretical predictions and practical applications. The research emphasized the importance of understanding NP interactions and processing conditions, providing a more comprehensive framework for optimizing NP materials. Despite these advancements, several challenges and research gaps remain. Prior work often neglected the holistic analysis of NPs, focusing instead on isolated properties or specific conditions. Additionally, optimal GO concentration and its effects under various environmental conditions were not well-established in the literature. This was while, the reliance on MD simulations, while valuable, required further validation via experimental studies to ensure real-world applicability. Furthermore, there was a need to explore how processing conditions, long-term stability, and interfacial interactions between polymer matrix and GO-NPs impact material performance.

2. Material and methods

2.1. Materials and reagents

This study explored the development and characterization of a SP-NCs comprising PU/PCL/GO-NC, with a focus on enhancing SM, MPs, and TPs through MD simulations. SM polymers were of great interest because of their potential uses in a variety of sectors. They were recognized for their ability to react to environmental stimuli including heat, light, electricity, and magnetism. The study leveraged the biocompatibility of PU-PCL and the unique TPs, electrical, and MPs of GO-NC to improve the performance of NCs. By incorporating these NPs, the material's responsiveness to external stimuli was accelerated, enabling activation via indirect thermal stimuli.

2.2. Details of present MD simulation

The research utilized a 300 Å SB to analyze the behavior of NCs, with VMD software [28] employed for simulation input and data analysis. Fig. 1 illustrates the atomic structure of NC sample subsequent to the equilibration process utilizing different amounts of GO-NPs. The graphical outcomes derived from MD simulations provided evidence that elevated ratios of GO-NPs did not introduce structural instability. Fig. 1 demonstrates that designed NCs remained physically stable in the presence of 5 % GO-NPs. As shown in Fig.1, blue particles represented nitrogen atoms, red particles represented oxygen atoms, white particles represented hydrogen atoms, and gray particles represented carbon atoms.

After the initial construction of model, the equilibrium of system was

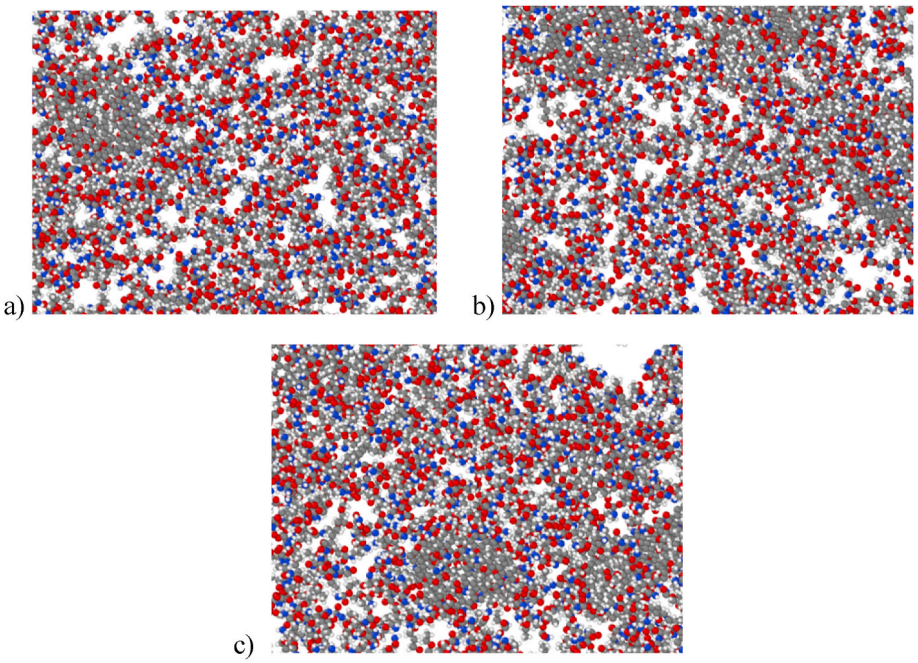

Fig. 1. Atomic structure modeled in the final step of equilibration process in the presence of a) 0.5, b) 2 and c) 5 % of GO. In these structures C, H, N, and O atoms presented by gray, white, blue, and red colours, respectively.

assessed. At this juncture, the NVT ensemble (constant Number of particles, Vol, and Temp) was applied to stabilize the system at target Temp = 300K. During this equilibration phase, key thermodynamic properties including the total system Temp, KE, and PE were meticulously monitored. Sampling was performed at the intervals of 20,000 time steps to ensure accurate data collection. The simulation was conducted with a time step resolution of 1 fs and a duration of 20 ns.The system achieved thermal equilibrium within the specified parameters by means of a 10-ns equilibration process. In scenarios where the system was assumed to be in thermal equilibrium and subject to constant Temp and pressure, NPT ensemble (constant Number of particles, Pressure, and Temp) was typically employed, particularly in the simulation of biological systems. In this ensemble, the number of particles, Temp, and pressure were held constant. To maintain these conditions, a Langevin thermostat was utilized to regulate Temp [29], while a Berendsen barostat was used to control the pressure [30].The results obtained from this section are given in Table 1. Finally to accurately simulate the bulk properties of material and eliminate edge effects, the study applied periodic boundary conditions (PBCs). Such circumstances provided the unlimited replication of the SB in all directions, hence establishing a continuous and seamless habitat for the particles. Upon surpassing one border of SB, a particle reemerges on the other side, therefore essentially simulating an endless system. This approach was essential for accurately representing bulk properties and minimizing surface artifacts that can arise in finite-sized simulations. The use of PBCs allowed the study to capture the material's behavior as if it were part of a larger, infinite system [31]. Technically, the conjugate gradient method used for energy optimization process to be done described MD simulations, correctly. This process was done until energy convergence reached 0.00001 eV. Furthermore, equilibrium phase simulations continued to 10 ns to detecting Temp and total energy convergence.

Table 1
A summary of the stopping criteria of this study.

Setting	Value
SB	$300 \times 300 \times 300$ Å^3
Boundary Condition	Periodically in 3 coordinate axes
Damping Temp	NVT&NPT ensembles
Time Steps	1 fs
Energy Minimization Method	Conjugate gradient
Simulation Time	20 ns

3. Results and discussion

Given the significance of SPs across various industries and the challenges related to their MPs and SM behavior, this study focused developing SP- NC consisting of PU/PCL/GO-NC. The study aimed to evaluate its SM, MPs, and TPs via MD simulations. Key metrics analyzed include.

- HF
- TC
- MSD
- Vol changes
- Stress-strain curves
- YM
- US
- T_g

These parameters were examined to understand the NPs behavior thoroughly. For this research, MD simulations at nanoscale were an appropriate and effective approach, providing results that were applicable to practical applications. MD simulation relies on three fundamental assumptions.

- The simulated structure was considered ideal and free of defects.
- Pressure was assumed to be uniform throughout the entire atomic system.
- Temp was uniformly maintained across the entire atomic system.

3.1. Results of the equilibration process

It was confirmed that the modeled structure was in equilibrium following the initial modeling. The necessary structure was initially equilibrated at 300 K, and a number of physical properties, including the

kinetic energy of simulated systems and the total Temp of simulated structures, were assessed. In Fig. 2, the temporal evolution of Temp throughout the atomic sample is depicted. Temp changes were observed during the initial phases of simulation, indicating that NPs were in motion and experiencing volatility within the simulated structure. The sample's Temp stabilized at 300 K after the simulation duration increased to 10 ns, indicating that the atomic structure had attained thermodynamic equilibrium [26]. The thermodynamic behavior of atomic samples decreased with time, indicating their stability. MD simulations continued to provide consistent findings in spite of metaphysical equilibrium condition. Furthermore, Temp's stability throughout the atomic sample indicated that 10 ns was a suitable simulation duration for this study.

To evaluate total behavior and stability of the sample, changes in kinetic energy were analyzed, as KE is directly related to Temp and thus provided insight into the system's thermal dynamics. KE stabilized at 0.9 kcal/mol after 10 ns, reflecting a steady thermal state and confirming the sample's stability. As atomic mobility decreased, this stabilization occurred, resulting in a reduction in oscillation amplitude and a more stable atomic configuration. The reduction in oscillations indicates that the system reached a thermodynamic equilibrium. The reduction in oscillations indicated that the system reached a thermodynamic equilibrium. Finally, to assess the thermodynamic equilibrium of simulated samples at 300 K, the potential energy of atomic structures was calculated. The results, depicted in Fig. 3, show that potential energy stabilized at 16.77 kcal/mol after 10 ns [26]. In this context, a negative potential energy value indicated strong interatomic attractions within the structure, suggesting that the atoms were well-bonded. The fact that the potential energy converged to a constant value indicated that the system reached thermodynamic equilibrium, which means that the atomic locations were stable and did not fluctuate significantly over time. This equilibrium reflected the system's total stability and implied that the simulated atomic sample was in a suitable and stable configuration for practical uses.

3.2. RDF

For a comprehensive structural analysis, the RDF of sample was calculated and is illustrated in Fig. 4. RDF provided a quantitative measure of atomic pair correlations within the material. In solid-phase structures, RDF displayed a series of sharp, periodic peaks, reflecting a regular, repeating atomic arrangement typical of crystalline or well-ordered materials. This periodicity characterized the atoms as being uniformly spaced and arranged in a coherent pattern. Within liquid-phase samples, RDF displayed a conspicuous peak at closer interatomic distances, suggesting the presence of local organization, followed by a sequence of decreasing peaks at ever greater distances. These smaller peaks eventually disappeared, which signified that while there was some degree of local atomic arrangement, long-range order was absent, properties of a disordered liquid structure. In gas-phase samples, response distribution function (RDF) showed a solitary peak at small distances, without any notable peaks seen at greater distances. Once the first peak was reached, RDF converged to a constant value, suggesting the absence of long-range atomic correlations. This observation aligned with the evident high level of disorder in gases. The RDF results for PU structure investigated in this study were consistent with previous reports, validating the accuracy of observed atomic arrangements. As RDF was a critical measure of the spatial distribution of atoms, these results confirm that MD simulation used was appropriate for accurately modeling the material's structural properties. This alignment with

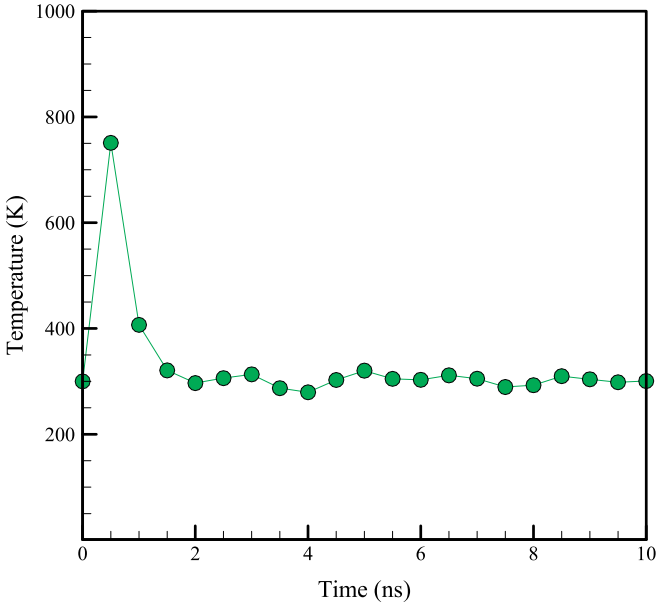

Fig. 2. Temp variations in the studied sample based on simulation time.

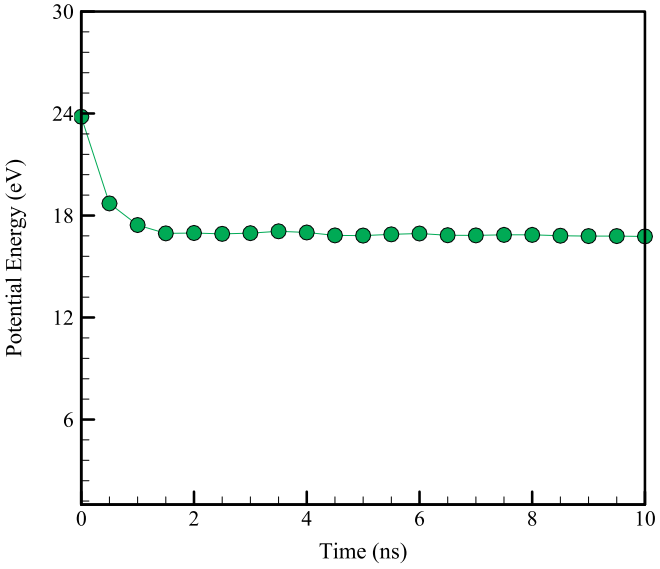

Fig. 3. PE variations in the studied sample based on simulation time.

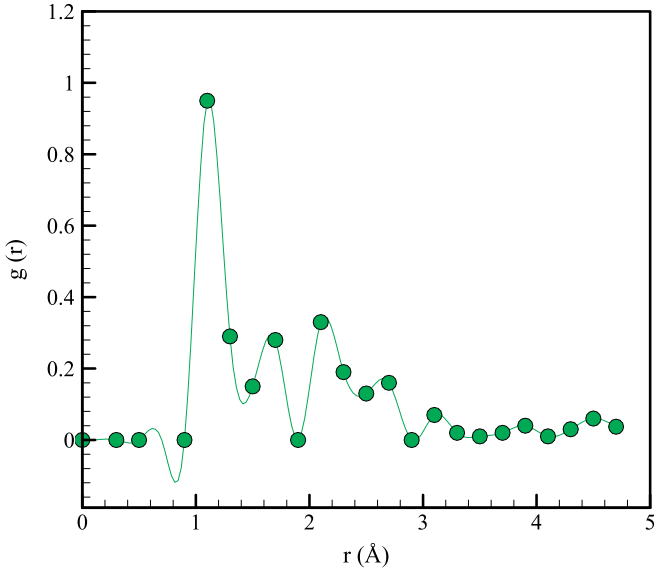

Fig. 4. RDF of PU in simulated atomic sample at 344 K.

established findings supported the reliability and effectiveness of computational methods used in this study [32].

3.3. Results related to MPs and TPs

LAMMPS software was used to analyze MPs, TPs, and SM propertiesof PU/PCL/GO polymer NCs in this phase of the research. The study calculated and reported the effects of different amounts of GO-NPs (0.5 %, 1 %, 2 %, and 5 %) on NC's TPs, MPs, and atomic properties. As GO-NP concentration affected the HF of PU/PCL/GO-NC sample manufactured at a pressure of 1 bar and a Temp = 300 K, Fig. 5 depicts the changes in HF. The results demonstrate that as GO-NP concentration increased, the HF in NC increased and reached its maximum value of 2 %. Specifically, increasing GO-NP concentration from 0.5 % to 2 % led to an increase in HF from 680.95 to 714.09 W/m^2. However, further increasing NP concentration to 5 % resulted in a decrease in HF from 714.09 to 705.82 W/m^2. Therefore, it can be concluded that the optimal TB for this investigated NC was achieved at a GO-NP concentration of 2 %. From a physical point of view, as the concentration of GO-NPs increased, the effective thermal pathways within the NCs enhanced, allowing for more efficient heat transfer via the material. Furthermore, additional NPs increase the frequency of interactions, which improved molecular energy transfer routes. At a concentration of 2 %, GO-NPs were dispersed optimally inside the polymer matrix, enhancing these thermal routes and resulting in the observed rise in HF. However, at higher concentrations, such as 5 %, GO-NP dispersion became less effective, resulting in agglomeration, which increases heat barriers and lowers total HF. This indicated that the TC benefits of GO-NPs were most effective at a specific concentration, beyond which increased particle concentration negatively affected heat transfer due to poor dispersion and resulting thermal losses.

TC of PU/PCL/GO-NC changed with GO-NP concentration, as shown in Fig. 6. The material was created Press = 1 bar and Temp = 300 K. According to MD modeling findings, higher HF levels lead to higher TC levels. As the concentration of GO-NPs grew from 0.5 % to 2 %, TC of the simulated NC increased from 0.69 W/m.K to 0.93 W/m.K. TC of the NC increased when GO-NPs with high TC were added to the base matrix. By adding more GO-NPs to the mixture until it reached a final concentration

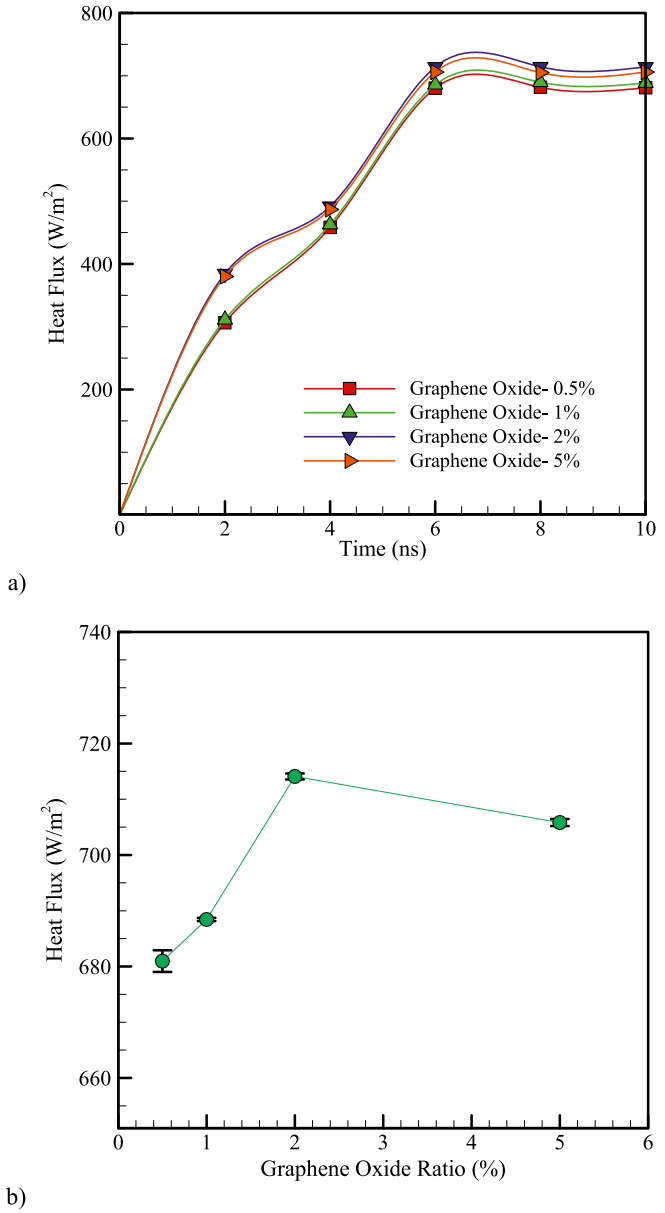

Fig. 5. The variations in the HF of designed NC based on passing a) simulation time and b)GO-NPs percentage.

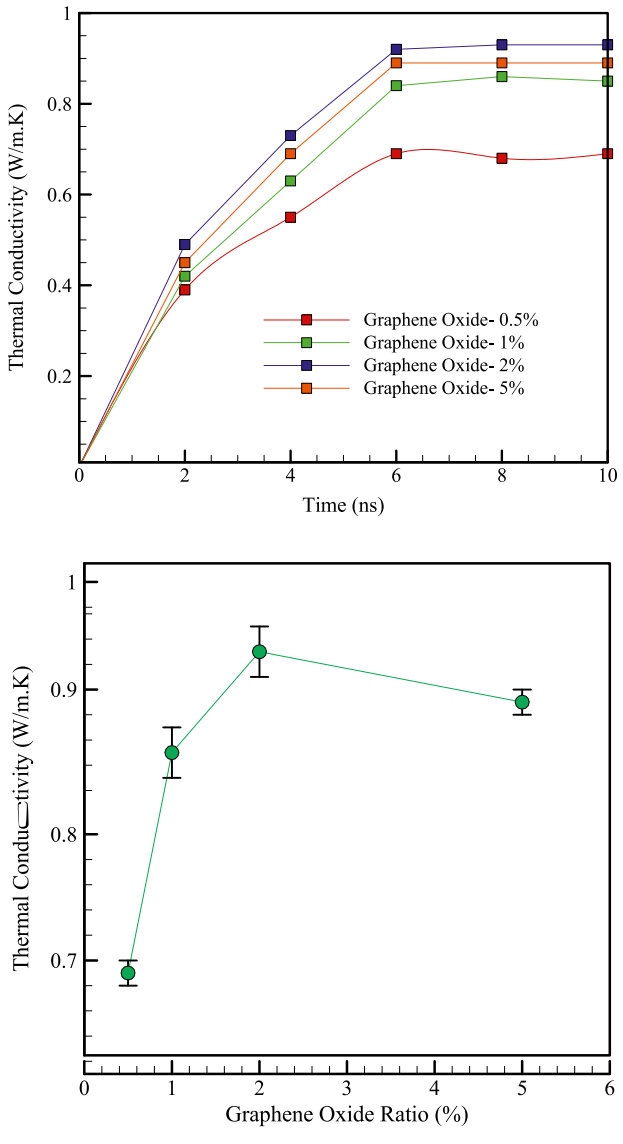

Fig. 6. The variations in the TC of designed NC based on passing a) simulation time and b)GO-NPs percentage.

of 5 %, the TC was lowered to 0.89 W/m.K. The reduction was caused by agglomeration and reduced TC as a consequence of the buildup and insufficient dispersion of NPs. The TC changes observed in the PU/PCL/GO-NC system, where TC initially increased from 0.69 W/m·K to 0.93 W/m·K as GO-NP concentration increased from 0.5 % to 2 %, can be explained by adding highly conductive GO-NPs, as predicted by models like Maxwell-Garnett and Bruggeman. Thus, following drop in TC to 0.89 W/m·K at 5 % GO-NP concentration is consistent with observations in the literature which was compatible with the occurrence of NP agglomeration, which lowered the effective thermal routes. Studies showed that beyond an optimal filler concentration, TC may decrease due to poor dispersion and aggregation of NPs, confirming that achieving a balance in GO-NP dispersion is crucial for optimizing TC in such composites [33].

In Fig. 7, the Vol changes of NC structure are depicted as a function of various atomic percentages of GO-NPs. The specific Vol values for GO-NP concentrations of 0.5, 1, 2, and 5 % were recorded as 27316, 27311, 27106, and 27101 nm^3, respectively, indicating a slight reduction in Vol as the concentration of GO-NPs increased (See Table 2). This steady convergence in Vol showed that adding more GO-NPs made the structure marginally more compact. On the other hand, the substantial Vol drop after increasing the GO-NP concentration from 0.5 % to 2.0 % was due to the first disruption of NPs matrix, where the new NPs efficiently fill gaps and pores, resulting in a denser structure. As more GO-NPs were introduced, they created additional bonding sites at the interfaces, causing the matrix to contract around the NPs. This effect became particularly significant as the concentration crosses a threshold, resulting in a more compact structure and a corresponding decrease in Vol. Physically, the small decrease in Vol by increasing GO-NP content suggested that NPs enhanced packing density and fill voids within the matrix, leading to a more tightly bound structure. Despite these changes, the structural integrity of NC remained largely intact, as indicated by the lack of significant deformation or destabilization in the graphical outputs and overall analysis. NC's minimal Vol decrease suggested that it can maintain its stability and rigidity even with higher percentages of GO-NPs, rendering it appropriate for applications that necessitate both strength and NP functionality. The convergence of Vol values suggested a saturation effect, where beyond a certain point, adding more GO-NPs did not significantly alter structure's Vol, highlighting the material's robustness.

Fig. 8 illustrates changes in the stress-strain diagram of PU/PCL/GO based on the quantity of GO-NPs used in the design. GO-NPs, due to their high aspect ratio and extensive surface area, provide efficient load transfer and reinforcement in the material, enhancing MPs including strength and stiffness. Additionally, GO-NPs act as obstacles to displacement movement, preventing plastic deformation and enhancing material resistance to deformation. Numerical results indicate that at a strain of 950 %, different concentrations of GO-NPs create various stress, and a numerical value of Us was equal to 72.59 MPa at a concentration of 2 % GO-NPs. In studies on PU/GO-NCs, adding 1–2% GO typically led to a significant increase in tensile strength, often within a comparable range, confirming efficient load transfer and reinforcement provided by GO-NPs [25,26]. The primary reason for observed reduction in stress after a certain strain in the PU/PCL/GO composites was the efficient load transfer and reinforcement provided by GO-NPs. Because of their large surface area and high aspect ratio, these NPs improved the mechanical properties of material by better dispersing the applied load and preventing plastic deformation by posing as barriers to dislocation movement. Consequently, material's resistance to deformation increased at larger strains, causing a brief increase in stress. However, beyond a certain strain level, the stress diminished as the material approached its US and began to experience failure. The observed trend in the numerical results, where higher GO-NP concentrations resulted in increased stress at high strains and enhanced resistance to plastic deformation, mirrors experimental findings, suggesting that the simulation model used accurately reflected the mechanical behavior (MB) of such NCs [34,35].

Fig. 9 illustrates the effect of various quantities of GO-NPs on the mechanical properties of a PU/PCL/GO-NC sample. The Fig. shows that the US of NC increased when GO-NP concentration raised from 0.5 % to 2 %, with the US rising from 55.89 MPa to 72.59 MPa. This improvement in MS was attributed to the enhanced interactions between GO-NPs and the polymer matrix. Specifically, at 2 % GO-NP concentration, the strong covalent bonding between GO-NPs and PU/PCL matrix improved total structural integrity and load-bearing capacity of composite, making it more robust and effective for practical applications. However, when the

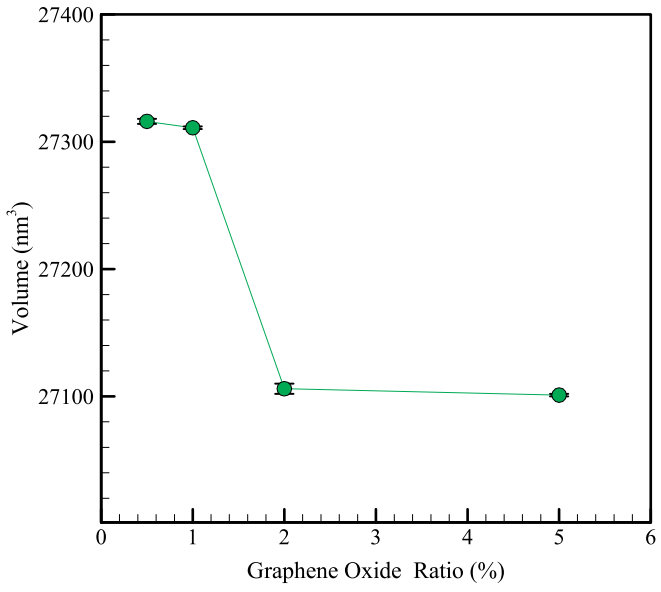

Fig. 7. Vol variations of the designed NC based on the amount of GO-NPs.

Table 2
Atomic and Thermal outputs of the simulated NC based on the amount of GO.

GO (%)	HF (W/m^2)	TC (W/m.K)	Vol (nm^3)
0.5	680.95 (±1.94)	0.69 (±0.01)	27316 (±2)
1	688.43 (±0.29) [26]	0.85 (±0.02) [26]	27311 (±1) [26]
2	714.09 (±0.54)	0.93 (±0.2)	27106 (±4)
5	705.82 (±0.63)	0.89 (±0.01)	27101 (±1)

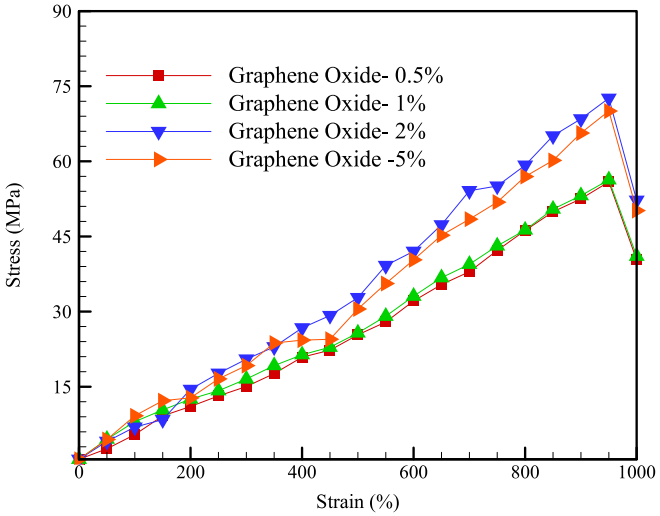

Fig. 8. The variations of stress-strain diagram in the designed NC based on the amount of GO-NPs.

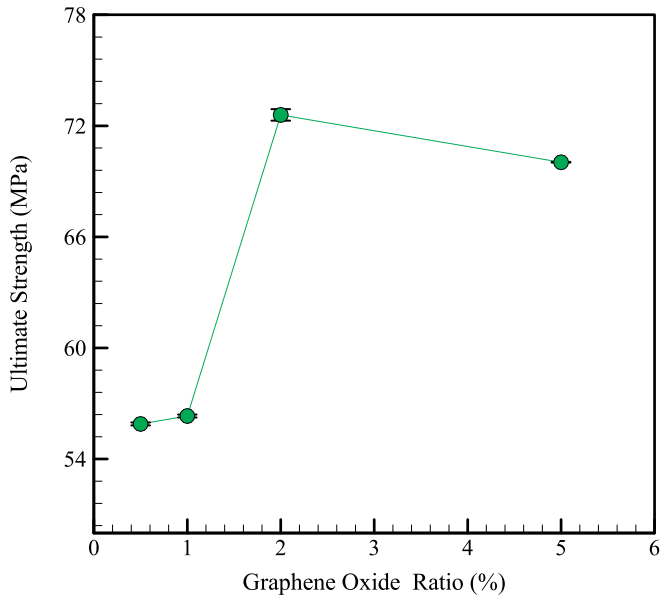

Fig. 9. US variations in the designed NC based on the amount of GO-NPs.

GO-NP concentration increased to 5 %, the US decreased to 70.03 MPa. This decrease in strength was likely due to NP agglomeration. At higher concentrations, GO-NPs tended to cluster together, forming aggregates that disrupt the uniform distribution within the matrix. This agglomeration can lead to weak points or voids within the NC, resulting in poorer mechanical performance. At higher concentrations, decreased adhesion and lack of proper interaction among the particles and the matrix diminished total MS. Thus, the optimal GO-NP concentration for maximizing mechanical performance in the PU/PCL/GO-NC is 2 %, where the balance between effective reinforcement and prevention of NPs clustering was achieved, ensuring both enhanced strength and structural stability.

Fig. 10 illustrates how the YM of PU/PCL/GO-NC changes with various concentrations of GO-NPs. As GO-NP concentration increased from 0.5 % to 2 %, YM increased from 5.91 to 6.63 MPa. This increase in YM reflected a stiffer material, attributed to strong covalent bonding between GO-NPs and the polymer matrix, which enhanced the composite's resistance to deformation under stress. From a physical perspective, the rise in YM with increased GO-NP concentration up to 2 % was due to the effective reinforcement provided by the NPs. GO-NPs integrated into the polymer matrix and improved load transfer and stress distribution, leading to a more rigid and elastic material. The strong contacts between GO-NPs and polymer chains led to the increased mechanical responsiveness seen in the higher YM. However, with a larger concentration of GO-NPs (5 %), the YM drops somewhat to 6.57 MPa. This drop was most likely due to NP agglomeration, in which excessive GO-NPs cluster together, disrupting uniform dispersion and generating areas with weak interfacial bonding. These aggregates can introduce defects and weak points within the matrix, reducing total stiffness and compromising the mechanical integrity of composite. This pattern of increase with moderate GO-NP addition and decrease with excessive GO-NPs parallels findings by Peng et al. [25], who observed similar decreases in YM with increasing Temp, and Heydari et al. [26], who reported improvements in YM with increased PCL content. The analysis reveals that the patterns in MPs examined in the present study align with previous research, indicating that ideal reinforcement and excessive concentrations affected mechanical performance.

Fig. 11 displays the mean square displacement (MSD) of NC with respect to GO-NPs. MSD and glass transition Temp (Tg) were critical properties that provided insights into the MD and structural behavior of NCs. MSD measures the average distance that atoms or molecules move over time, which is closely linked to the material's mobility and, consequently, its MPs and TPs. The inclusion of GO-NPs in PU/PCL/GO-NC material had a substantial effect on its properties, mainly because of the robust interactions between polymer matrix and GO-NPs. The incorporation of GO-NPs into the polymer matrix resulted in their interaction with the adjacent polymer chains, therefore limiting their mobility and consequently decreasing MSD. This is because the rigid GO-NPs imposed constraints on the motion of polymer chains, leading to a more confined molecular environment. The decrease in MSD from 0.26 to 0.22 $Å^2$ when increasing GO-NP content from 0.5 % to 2 % reflected this enhanced interaction and reduced molecular mobility. This reduced mobility was associated with a decrease in Tg, observed at 318 K, as the NPs disrupt the polymer's molecular arrangement, limiting the cooperative segmental motions necessary for the glass transition. However, as the concentration of GO-NPs increased further to 5 %, the MSD increased slightly to 0.24 $Å^2$. This was due to the aggregation or clumping of GO-NPs at greater concentrations, resulting in less efficient

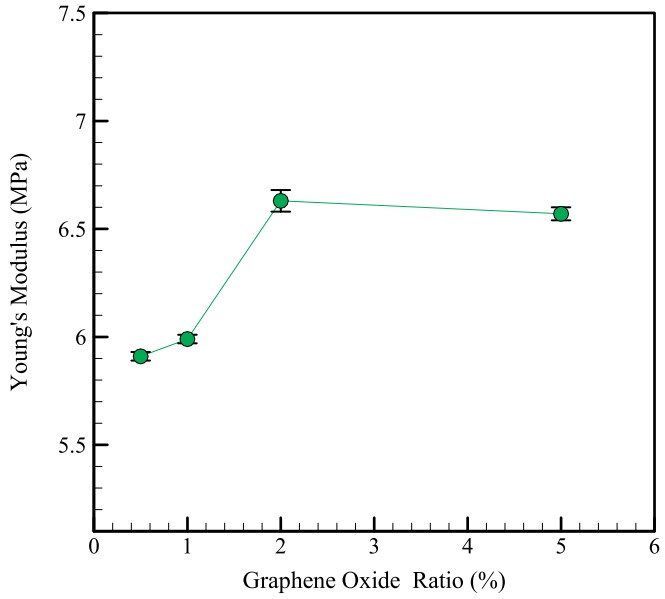

Fig. 10. The variations of YM in designed NC based on the amount of GO-NPs.

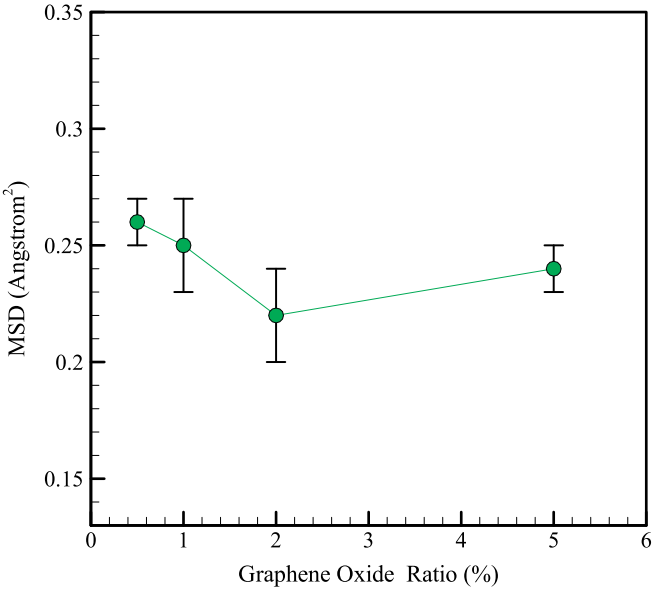

Fig. 11. The variations of MSD in the designed NC sample based on the amount of GO-NPs.

interaction with polymer chains. In addition, the aggregation of NPs resulted in a repulsive force among them according to Pauli exclusion principle. This structural method reduced the mechanical stability (mechanical strength) of the whole system to a lower level. These aggregates create regions within the NCs where the polymer chains can move more freely, partially restoring the mobility and thus increasing MSD. This behavior highlighted the delicate balance between NPs dispersion and aggregation, which critically affected the MD and total properties of NCs. Understanding these relationships was essential for optimizing MPs and TPs of NCs by fine-tuning the NPs content and distribution.

Table 3 presents the relationship between the quantity of GO-NPs and MPs (US and YM, MSD parameter), and Tg of PU/PCL/GO-NC modeled at a Temp = 300 K and a pressure of 1 bar.

4. Conclusion

The TB and MB of PU/PCL/GO was examined using MD simulation methods. The main computational package consisted of LAMMPS, supplementary modeling, and graphics software. A portion of the simulations utilized in this study were devoted to the analysis and equilibrium of atomic structures, as well as the investigation of their atomic, MPs, and thermodynamic properties. In order to accomplish this, simulated samples were first equilibrated at 300 K and 1 bar of pressure for 10 ns. A concise summary of the study's findings is as follows.

- The initial simulated system reached convergence at 300 K after 10 ns, indicating that the simulation settings were correct and sufficient for this study.
- The PE of particles within the SB converged to a certain value of 16.77 kcal/mol.
- Adding GO-NPs improved TB and MB of designed structure, with optimal results observed when using 2 % NPs.
- Increasing the concentration of GO-NPs from 0.5 % to 2 % resulted in an increase in HF from 680.95 to 714.09 W/m^2. However, when the concentration increased to 5 %, HF decreased to 705.82 W/m^2.
- The increase in GO-NP concentration from 0.5 % to 2 % led to an increase in TC of the simulated NC from 0.69 to 0.93 W/m.K. However, with a further increase in NP concentration, the TC reached 0.89 W/m.K.
- Increasing the concentration of GO-NPs from 0.5 % to 2 % resulted in an increase in YM of the simulated NC from 5.91 to 6.63 MPa.
- Adding more NPs caused lumpiness and reduced the MS of the NC due to a lack of correlation and proper adhesion among the particles.
- Increasing the concentration of GO-NPs from 0.5 % to 2 % resulted in a decrease in MSD from 0.26 to 0.22 Å^2.
- The presence of NPs limited particle movement and decreased displacement and MSD, according to the obtained results.

These findings suggest that PU/PCL/GO-NCs with optimal GO-NP concentrations (around 2 %) offer promising advancements in several applications. These materials are suitable for thermal insulation and thermal management in electronics due to their improved thermal conductivity. However, enhanced MPs could be advantageous in biomedical devices, aerospace structural components, and high-performance coatings, where thermal stability and strength are essential. The controlled addition of GO-NPs can thus lead to advanced NCs materials with tailored properties for a wide range of industrial and technological applications. However, it should be noted that, the MD simulations provided valuable insights into the TB and MB of PU/PCL/GO-NCs, but have limitations, including small system sizes, short simulation times, and reliance on idealized conditions that may not account for real-world complexities. To address these limitations, future research should use larger system sizes, longer simulation times, and include experimental validation. Moreover, using advanced simulation techniques and considering real-world processing conditions could further enhance the understanding of NCs practical applications and performance.

CRediT authorship contribution statement

Shapour Fadaei Heydari: Software, Data curation. **Mohamad Shahgholi:** Writing – original draft, Supervision. **Arash Karimipour:** Writing – review & editing, Validation. **Mehdi Salehi:** Visualization. **Seyed Ali Galehdari:** Project administration, Methodology.

Declaration of competing interest

The authors declare that they have no known competing financial interests or personal relationships that could have appeared to influence the work reported in this paper.

Data availability

Data will be made available on request.

Appendix

The computational method of MD simulation was utilized to examine the temporal behavior and interactions of atoms and molecules. It was used across diverse scientific fields to acquire comprehension of intricate systems operating at the molecular and atomic levels. By calculating the equations of motion for each particle in a system numerically, researchers may examine particle interactions and monitor the location and velocity of the particles over time to comprehend thermodynamic characteristics and system dynamics. The current research utilized comprehensive simulation software LAMMPS based on the MD simulation methods [36–39]. LAMMPS is a robust software application that provides an extensive array of force fields and simulation methodologies. These functionalities enable researchers to perform simulations on a significant scale and scrutinize intricate systems [40,41]. Newton's second law, which establishes an equation connecting force, acceleration, and particle mass, serves as the foundation for the MD simulations in LAMMPS [42,43]:

$$F_i = \sum_{i \neq j} F_{ij} = m_i \frac{d^2 r_i}{dt^2} = m_i \frac{dv_i}{dt} \quad \text{(a-1)}$$

On the other hand, F_i is obtained from the negative derivative of potential function U [42]:

$$F_i = -\nabla U_i = -\frac{\partial U}{\partial r_i} \quad \text{(a-2)}$$

Verlet-Velocity algorithm was commonly used in MD simulations to calculate particle positions and Velocities over time. This numerical integration method updates particle positions and velocities based on

Table 3
Atomic, and mechanical outputs of simulated NC based on the amount of GO.

GO (%)	US (MPa)	YM (MPa)	MSD (Å^2)	T$_g$ (K)
0.5	55.89 (±0.08)	5.91 (±0.02)	0.26 (±0.01)	324 (±2)
1	56.32 (±0.08) [26]	5.99 (±0.02) [26]	0.25 (±0.02) [26]	321 (±2) [26]
2	72.59 (±0.03)	6.63 (±0.05)	0.22 (±0.02)	318 (±2)
5	70.03 (±0.02)	6.57 (±0.03)	0.24 (±0.01)	320 (±1)

current values and acting forces, resulting in accuracy and stability. This type of algorithm is known for its accuracy in preserving the energy of the entire system, which is very important in the MD simulation. It is also numerically stable. This signified that the model generated dependable and consistent outcomes, even when simulating intricate and particle-laden systems. A synopsis of the formulation of this type of algorithm follows [44, 45]:

$$r_i(t+\Delta t) = r_i(t) + \Delta t\, v_i(t) + \frac{\Delta t^2 a_i\,(t)}{2} \tag{a-3}$$

$$v_i(t+\Delta t) = v_i(t) + \Delta t\, a_i(t) + \frac{\Delta t\,(a_i\,(t) + a_i(t+\Delta t))}{2} \tag{a-4}$$

$r_i(t)$ and $v_i(t)$ indicates the position and Velocity of particles in the time step (t). The position $r_i(t+\delta t)$ and Velocity $v_i(t+\delta t)$ of the particles can be calculated in the next steps using the corresponding values in the previous step.

Defining the desired system, including the quantities and types of particles, their initial positions, and Velocities, in addition to any limitations or boundary conditions, is the initial phase in the MD simulation. The system's scale can vary from a single molecule to an entire solid. The mathematical representation of particle interactions within a system is a force field. The framework includes terms for potential energy components in addition to bonding interactions (e.g., covalent bonds) and nonbonding interactions (e.g., van der Waals forces and electrostatic interactions). The selection of the force field is determined by the intended degree of precision and the properties of the system. The fact that LAMMPS provides access to a variety of force fields for distinct particle types and systems is one of its benefits. Force fields are essential components in MD simulations as they guarantee the precise representation of atomic and molecular interactions. They provide the essential data required for the calculation of forces exerted on individual atoms, which ultimately dictate the system's temporal behavior. The LJ and Coulomb force fields were used in this specific investigation to characterize the interactions between particles within the system under investigation. LJ potential takes van der Waals interactions among elements into account.

It is characterized by two parameters: well depth (ε_{ij}), representing interaction strength, and the equilibrium distance at which potential energy was zero (σ_{ij}) [46,47]:

$$U_{LJ} = 4\varepsilon\left[\left(\frac{\sigma}{r}\right)^{12} - \left(\frac{\sigma}{r}\right)^{6}\right] r < r_c \tag{a-5}$$

In this study, a r_c of 12 Å is employed for calculating non-bonded interactions, such as van der Waals and electrostatic forces. This radius defines the maximum distance at which interactions between particles are considered. By setting a cutoff of 12 Å, the simulation balances computational efficiency with accuracy, ensuring that interactions are calculated only within this specified range. This choice helps manage the computational load while maintaining a reasonable level of precision for the interaction energies and forces.

$$\varepsilon_{ij} = \sqrt{\varepsilon_i \varepsilon_j} \tag{a-6}$$

$$\sigma_{ij} = \frac{\sigma_i + \sigma_j}{2} \tag{a-7}$$

On the other hand, Coulomb interactions consider the electrostatic forces among charged particles which are described by the equation of Coulomb's law [51]:

$$U_{ij}(r) = \frac{-1}{4\pi\varepsilon_0}\frac{q_i q_j}{{r_{ij}}^2} \tag{a-8}$$

Table a-1
LJ potential function parameters of the present particles [48,49].

Particles	ε (kcal/mol)	σ (Å)
H	0.01	3.20
O	0.415	3.71
C	0.3050	4.18
N	0.415	3.995

The values of σ and ε of each interaction among the particles were calculated using Eqs. a-6 and a-7 [50].

The accuracy of MD simulations for PU/PCL-NCs with GO-NPs is heavily influenced by the choice of force fields, specifically LJ and Coulomb interactions [26]. The van der Waals forces are effectively captured by the LJ potential, which is essential for accurately modeling the non-bonded interactions between the polymer matrix and the GO surface. This directly affects the predictions of MPs, such as modulus and tensile strength. Meanwhile, the Coulomb potential is essential for accounting for electrostatic interactions, especially given the partial charges on GO's functional groups, which significantly affect NCs TPs, such as heat capacity and TC. An imbalance or inaccurate parameterization of these force fields could lead to erroneous predictions of the MPs and TB of the NCs, underscoring the need for careful selection and calibration to ensure reliable simulation results.

References

[1] C.S. Brazel, S.L. Rosen, Fundamental Principles of Polymeric Materials, John Wiley & Sons, 2012.
[2] R.F. Landel, L.E. Nielsen, Mechanical Properties of Polymers and Composites, CRC press, 1993.
[3] Saina Alasvandian, Mohamad Shahgholi, Arash Karimipour, Investigating the effects of chitosan atomic ratio and drug type on mechanical properties of silica

aerogel/chitosan nanocomposites using molecular dynamics approach, J. Mol. Liq. 401 (2024) 124639.
[4] J.G. Drobny, Polymers for Electricity and Electronics: Materials, Properties, and Applications, John Wiley & Sons, 2012.
[5] N.A.M. Radzuan, A.B. Sulong, J. Sahari, A review of electrical conductivity models for conductive polymer composite 42 (14) (2017) 9262–9273.
[6] B. Gong, et al., Magnetic Field-Responsive Smart Polymer Composites, 2007, pp. 137–189.
[7] L. Jingcheng, V.S. Reddy, W.A. Jayathilaka, A. Chinnappan, S. Ramakrishna, R. Ghosh, Intelligent polymers, fibers and applications 13 (9) (2021) 1427.
[8] H. Palza, P.A. Zapata, C. Angulo-Pineda, Electroactive smart polymers for biomedical applications 12 (2) (2019) 277.
[9] J. Hu, Y. Zhu, H. Huang, J. Lu, Recent advances in shape–memory polymers: structure, mechanism, functionality, modeling and applications 37 (12) (2012) 1720–1763.
[10] A. Lendlein, S. Kelch, Shape-memory polymers 41 (12) (2002) 2034–2057.
[11] J. Leng, X. Lan, Y. Liu, S. Du, Shape-memory polymers and their composites: stimulus methods and applications 56 (7) (2011) 1077–1135.
[12] J. Hu, Shape Memory Polymers and Textiles, Elsevier, 2007.
[13] A. Mitchell, U. Lafont, M. Hołyńska, C. Semprimoschnig, Additive Manufacturing—A Review of 4D Printing and Future Applications, vol. 24, 2018, pp. 606–626.
[14] R. Fada, M. Shahgholi, R. Azimi, et al., Estimation of porosity effect on mechanical properties in calcium phosphate cement reinforced by strontium nitrate nanoparticles: fabrication and FEM analysis, Arab J Sci Eng 49 (2024) 1815–1825.
[15] M. Mahjoory, M. Shahgholi, A. Karimipour, "investigation on the Size and percentage Effects of magnesium Nanoparticles on thermophysical Properties of reinforced calcium phosphate bone Cement by molecular dynamic simulation", Heliyon 9 (2023) e18835.
[16] E. Archer, M. Torretti, S. Madbouly, "Biodegradable Polycaprolactone (PCL) Based Polymer and Composites,", 2021 no. 0, p. 000010151520200074.
[17] D. Razzaghi, M. Rezaei, A. Babaie, The Effect of Incorporating Graphene and Polycaprolactone-Grafted Graphene Oxide Nanosheets on Thermal and Physico-Mechanical Properties, Microstructure and Biocompatibility of Electrospun Polyurethane Nanocomposite Mats, vol. 224, 2021 109210.
[18] F. Azadi, S.H. Jafari, H.A. Khonakdar, M. Arjmand, U. Wagenknecht, V. Altstädt, "Influence of graphene oxide on thermally induced shape memory behavior of PLA/TPU blends: correlation with morphology, creep behavior, crystallinity, and dynamic mechanical properties," 306 (2) (2021) 2000576.
[19] B. Cetiner, G. Sahin Dundar, Y. Yusufoglu, B. Saner Okan, Sustainable engineered design and scalable manufacturing of upcycled graphene reinforced polylactic acid/polyurethane blend composites having shape memory behavior 15 (5) (2023) 1085.
[20] G. Liang, et al., Improvement of mechanical properties and solvent resistance of polyurethane coating by chemical grafting of graphene oxide 15 (4) (2023) 882.
[21] A. Gupta, T.H. Mekonnen, Cellulose Nanocrystals Enabled Sustainable Polycaprolactone Based Shape Memory Polyurethane Bionanocomposites, vol. 611, 2022, pp. 726–738.
[22] T. Saidi, M. Hasan, Z. Amalia, S. Salsabila, The analysis of the bond strength between natural fiber reinforced polymer (NFRP) sheets and concrete, Results in Engineering 18 (2023) 101124.
[23] M. Samuel, R.B. Tayong, 3D numerical analysis of the structural behaviour of a carbon fibre reinforced polymer drive shaft, Results in Engineering 18 (2023) 101120.
[24] M.A. Karim, M.Z. Abdullah, A.F. Deifalla, M. Azab, A. Waqar, An assessment of the processing parameters and application of fibre-reinforced polymers (FRPs) in the petroleum and natural gas industries: a review, Results in Engineering 18 (2023) 101091.
[25] S. Peng, Y. Geng, Z. Li, S.F. Heydari, M. Shahgholi, Investigating the effects of temperature on thermal and mechanical properties of polyurethane/polycaprolactone/graphene oxide nanocomposites: focusing on creating a smart polymer nanocomposite via molecular dynamics method, Mol. Phys. (2024) e2351164.
[26] S.F. Heydari, M. Shahgholi, M. Salehi, S.A. Galehdari, Effect of polycaprolactone percentage on thermal and mechanical behavior of polyurethane/polycaprolactone/graphene oxide nanocomposite utilizing molecular dynamics simulation, Eng. Anal. Bound. Elem. 161 (2024) 179–187.
[27] W. Quanguo, Y. Ke, C. Qingli, Molecular simulation investigations on the interaction properties of graphene oxide-reinforced polyurethane nanocomposite toward the improvement of mechanical properties, Mater. Today Commun. 35 (2023) 106404.
[28] W. Humphrey, A. Dalke, K. Schulten, VMD: visual molecular dynamics, J. Mol. Graph. 14 (1) (1996) 33–38.
[29] T. Panczyk, T. Da Ros, G. Pastorin, A. Jagusiak, J. Narkiewicz-Michalek, Role of intermolecular interactions in assemblies of nanocontainers composed of carbon nanotubes and magnetic nanoparticles: a molecular dynamics study, J. Phys. Chem. C 118 (2) (2014) 1353–1363.
[30] Y.-F. Xing, C.-L. Yang, Y.-F. Mo, M.-S. Wang, X.-G. Ma, Dynamic mechanism of single-stranded DNA encapsulated into single-wall carbon nanotubes: a molecular dynamics simulation study, J. Phys. Soc. Jpn. 83 (2) (2014) 024801.
[31] L. Jaillet, S. Artemova, S. Redon, IM-UFF: extending the universal force field for interactive molecular modeling, J. Mol. Graph. Model. 77 (2017) 350–362.
[32] W.F. Gum, W. Riese, H. Ulrich, Reaction polymers: polyurethanes, epoxies, unsaturated polyesters, phenolics, special monomers, and additives: chemistry, technology, applications, markets, (No Title) (1992).
[33] H. Im, J. Kim, Thermal conductivity of a graphene oxide–carbon nanotube hybrid/epoxy composite, Carbon 50 (15) (2012) 5429–5440.
[34] X. Zhao, Mechanical Properties of Graphene and Graphene-Based Nanocomposites, The University of Manchester, United Kingdom, 2018.
[35] D.G. Papageorgiou, I.A. Kinloch, R.J. Young, Mechanical properties of graphene and graphene-based nanocomposites, Prog. Mater. Sci. 90 (2017) 75–127.
[36] M.S. Badar, S. Shamsi, J. Ahmed, M.A. Alam, Molecular dynamics simulations: concept, methods, and applications, in: Transdisciplinarity, Springer, 2022, pp. 131–151.
[37] W.F. Van Gunsteren, H.J. Berendsen, Computer simulation of molecular dynamics: methodology, applications, and perspectives in chemistry 29 (9) (1990) 992–1023.
[38] B. Leimkuhler, C. Matthews, Molecular Dynamics, vol. 39, 2015, p. 443.
[39] S.A. Hollingsworth, R.O. Dror, Molecular dynamics simulation for all 99 (6) (2018) 1129–1143.
[40] A.P. Thompson, et al., "LAMMPS-a flexible simulation tool for particle-based materials modeling at the atomic, meso, and continuum scales," 271 (2022) 108171.
[41] K. Vollmayr-Lee, Introduction to molecular dynamics simulations 88 (5) (2020) 401–422.
[42] D.C. Rapaport, The Art of Molecular Dynamics Simulation, Cambridge university press, 2004.
[43] D.C. Rapaport, D.C.R. Rapaport, The Art of Molecular Dynamics Simulation, Cambridge university press, 2004.
[44] S. Sarkar, R.P. Selvam, Molecular dynamics simulation of effective thermal conductivity and study of enhanced thermal transport mechanism in nanofluids, J. Appl. Phys. 102 (7) (2007/10/01 2007) 074302, https://doi.org/10.1063/1.2785009.
[45] D. McQuarrie, Statistical Mechanics, university science books, 2000, pp. 222–223.
[46] A. Oluwajobi, X. Chen, The effect of interatomic potentials on the molecular dynamics simulation of nanometric machining, Int. J. Autom. Comput. 8 (3) (2011) 326.
[47] N. Von Solms, R. O'Lenick, Y. Chiew, Leonard-Jones chain mixtures: variational theory and Monte Carlo simulation results, Mol. Phys. 96 (1) (1999) 15–29.
[48] A.K. Rappé, C.J. Casewit, K. Colwell, W.A. Goddard III, W.M. Skiff, UFF, a full periodic table force field for molecular mechanics and molecular dynamics simulations, J. Am. Chem. Soc. 114 (25) (1992) 10024–10035.
[49] S.L. Mayo, B.D. Olafson, W.A. Goddard, DREIDING: a generic force field for molecular simulations, Journal of Physical chemistry 94 (26) (1990) 8897–8909.
[50] H. Berendsen, J. Grigera, T. Straatsma, The missing term in effective pair potentials, J. Phys. Chem. 91 (24) (1987) 6269–6271.
[51] P.G. Huray, Maxwell's Equations, John Wiley & Sons, 2011.